IV International Conference on Computational Methods for Coupled Problems in Science and Engineering
COUPLED PROBLEMS 2011
M. Papadrakakis, E. Oñate and B. Schrefler (Eds)

A REFINED 1D FE MODEL FOR THE APPLICATION TO AEROELASTICITY OF COMPOSITE WINGS

Alberto Varello*†, Marco Petrolo*† and Erasmo Carrera*

*Department of Aeronautic and Space Engineering, Politecnico di Torino
Corso Duca degli Abruzzi 24, 10129 Torino, Italy
e-mail: erasmo.carrera@polito.it, www.mul2.com

†Institut Jean Le Rond d'Alembert, UMR 7190 CNRS, Univ Paris 6
Case 162, Tour 55-65, 4, Place Jussieu, 75252 Paris, France
e-mail: alberto.varello@polito.it, www.mul2.com

Key words: Aeroelasticity, FE-VLM Coupling, Refined Beam Models, Composite Wings, Unified Formulation

Abstract. The extension of a hierarchical one-dimensional structural model to aeroelasticity is the subject of the present paper. The aerodynamic model is based on the Vortex Lattice Method, VLM, whereas the refined 1D model is based on the Carrera Unified Formulation, CUF. Airfoil in-plane deformation and warping are introduced by enriching the displacement field over the cross-section of the wing. Linear to fourth-order expansions are adopted and classical beam theories (Euler-Bernoulli and Timoshenko) are obtained as particular cases. The VLM aerodynamic theory is coupled with the structural finite element model via an appropriate adaptation of the Infinite Plate Spline method. The aeroelastic tailoring is investigated for several wing configurations (by varying aspect ratio, airfoil geometry and sweep angle) and an excellent agreement with MD NASTRAN solution is provided for structural and aeroelastic cases. The effectiveness of higher-order models for an accurate evaluation of aeroelastic response of isotropic and composite wings is shown.

1 INTRODUCTION

Composite materials are widely used nowadays in a large variety of applications and engineering fields. The advantages related to their spread are becoming so significant that composites are by now a must for state-of-the-art manufacturing technology.

The requirements of weight saving and structural efficiency for aerospace systems such as rotor blades, aircraft wings, and helicopter rotor blades are leading to a wide use of structures in the form of composite thin-walled beams. This makes the accurate evaluation of the response of deformable lifting bodies (LBs) when subjected to steady and unsteady

aerodynamic loadings an even more challenging issue for the aeroelastic design of aerospace vehicles [8]. Over the last decades, many significant contributions have been given in structural, aerodynamic, and aeroelastic coupling modeling [12]. A relevant review article about recent advances in describing fluid-structure interaction is found in Dowell and Hall [9].

Composite beam-like structures can be analyzed by means of beam models provided that a number of non-classical effects such as large torsional warping are incorporated. Detailed structural and aeroelastic models are essential to fully exploit non-classical effects in design due to the properties characterizing advanced composite material structures, such as anisotropy, heterogeneity and transverse shear flexibility [14]. A detailed review of the recent development of beam models can be found in [20]. A considerable amount of work was done in trying to improve the global response of classical beam theories [11, 19] using appropriate shear correction factors, as described by Timoshenko [19]. El Fatmi [10] improved on the displacement field over the beam cross-section by introducing a warping function to refine the description of normal and shear stress of the beam. An asymptotic type expansion in conjunction with variational methods (VABS) was proposed by Yu and co-workers [22]. Generalized beam theories (GBT) have improved classical theories by using a piece-wise beam description of thin-walled sections [18].

Among the various extensions of refined beam models to aeroelasticity, the work done by Librescu and Song [16] on divergence instability of swept-forward wings made of composite materials is mentioned. A thin-walled beam model was implemented which incorporated the anisotropy of the material, transverse shear deformation and warping effects.

Carrera and co-authors have recently proposed refined 1D theories with only generalized displacement variables for the analysis of compact and thin-walled sections/airfoils. Higher-order finite elements are obtained in the framework of the Carrera Unified Formulation, CUF, which considers the order of the model as a free-parameter of the analysis. This technique has been developed over the last decade for plate/shell models [2] and it has recently been extended to beam static and dynamic modeling [4, 5, 6].

The present work couples a refined 1D model based on CUF with the Vortex Lattice Method (VLM) for the analysis of static aeroelastic response of aircraft wings. The aerodynamic load transferring is based on the work presented by Demasi and Livne [8] via the Infinite Plate Spline method [13]. In the proposed formulation (see Varello et al.[21]), the computation of linear steady aerodynamic loads refers to the VLM presented by Katz and Plotkin [15].

2 PRELIMINARIES

A beam-like structure with axial length L is considered. A local cartesian coordinate system is defined in Fig. 1. The cross-section of the structure is Ω and the beam longitudinal axis is along the y direction. The displacement vector of a generic point is:

$$\boldsymbol{u}\left(x,\, y,\, z\right) \;=\; \left\{ \begin{array}{ccc} u_x & u_y & u_z \end{array} \right\}^T \tag{1}$$

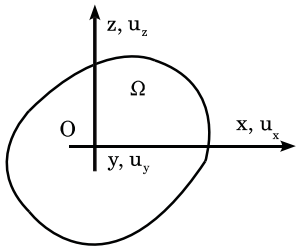

Figure 1: Beam's cross-section geometry and coordinate system.

The stress, $\boldsymbol{\sigma}$, and the strain, $\boldsymbol{\varepsilon}$, are grouped in vectors as follows:

$$\begin{aligned} \boldsymbol{\sigma}_p &= \left\{ \sigma_{zz} \quad \sigma_{xx} \quad \sigma_{zx} \right\}^T & \boldsymbol{\varepsilon}_p &= \left\{ \varepsilon_{zz} \quad \varepsilon_{xx} \quad \varepsilon_{zx} \right\}^T \\ \boldsymbol{\sigma}_n &= \left\{ \sigma_{zy} \quad \sigma_{xy} \quad \sigma_{yy} \right\}^T & \boldsymbol{\varepsilon}_n &= \left\{ \varepsilon_{zy} \quad \varepsilon_{xy} \quad \varepsilon_{yy} \right\}^T \end{aligned} \tag{2}$$

The subcripts n and p refer to quantities related to the cross-section Ω and the out-of-plane direction, respectively. In case of small displacements with respect to the length L, the linear strain-displacement relationships hold and are written in a compact notation:

$$\begin{aligned} \boldsymbol{\varepsilon}_p &= \boldsymbol{D}_p \, \boldsymbol{u} \\ \boldsymbol{\varepsilon}_n &= \boldsymbol{D}_n \, \boldsymbol{u} = \boldsymbol{D}_{np} \, \boldsymbol{u} + \boldsymbol{D}_{ny} \, \boldsymbol{u} \end{aligned} \tag{3}$$

where $\boldsymbol{D}_p$, $\boldsymbol{D}_{np}$, and $\boldsymbol{D}_{ny}$ are differential matrix operators. Constitutive laws are introduced for beams made of linear elastic orthotropic materials:

$$\begin{aligned} \boldsymbol{\sigma}_p &= \widetilde{\boldsymbol{C}}_{pp} \, \boldsymbol{\varepsilon}_p + \widetilde{\boldsymbol{C}}_{pn} \, \boldsymbol{\varepsilon}_n \\ \boldsymbol{\sigma}_n &= \widetilde{\boldsymbol{C}}_{pn}^T \, \boldsymbol{\varepsilon}_p + \widetilde{\boldsymbol{C}}_{nn} \, \boldsymbol{\varepsilon}_n \end{aligned} \tag{4}$$

where matrices $\widetilde{\boldsymbol{C}}_{pp}$, $\widetilde{\boldsymbol{C}}_{pn}$, and $\widetilde{\boldsymbol{C}}_{nn}$ are:

$$\widetilde{\boldsymbol{C}}_{pp} = \begin{bmatrix} \widetilde{C}_{11} & \widetilde{C}_{12} & 0 \\ \widetilde{C}_{12} & \widetilde{C}_{22} & 0 \\ 0 & 0 & \widetilde{C}_{44} \end{bmatrix}, \; \widetilde{\boldsymbol{C}}_{pn} = \begin{bmatrix} 0 & \widetilde{C}_{16} & \widetilde{C}_{13} \\ 0 & \widetilde{C}_{26} & \widetilde{C}_{23} \\ \widetilde{C}_{45} & 0 & 0 \end{bmatrix}, \; \widetilde{\boldsymbol{C}}_{nn} = \begin{bmatrix} \widetilde{C}_{55} & 0 & 0 \\ 0 & \widetilde{C}_{66} & \widetilde{C}_{36} \\ 0 & \widetilde{C}_{36} & \widetilde{C}_{33} \end{bmatrix} \tag{5}$$

For the sake of brevity, the dependence of the coefficients $\widetilde{C}_{ij}$ on Young's moduli, Poisson's ratios, shear moduli, and the fiber orientation angle θ is not reported here. It can be found in the book by Reddy [17]. θ is defined as the angle from the x axis to the 1-material axis on the $x-y$ plane.

3 REFINED ONE-DIMENSIONAL THEORY AND FE FORMULATION

According to the framework of the CUF [2, 7], the displacement field is assumed to be an expansion of generic functions F_τ, which depend on the cross-section coordinates x and z:

$$\boldsymbol{u}\,(x,\, y,\, z) \;=\; F_\tau\,(x,\, z)\,\boldsymbol{u}_\tau\,(y) \qquad\qquad \tau = 1,\; 2,\; \ldots\,,\; N_u \;=\; N_u\,(N) \tag{6}$$

The number of terms N_u depends on the expansion order N, which is a free parameter of the formulation. Mac Laurin's polynomials $x^i z^j$ are chosen as cross-section functions F_τ and hence Eq. 6 is a Taylor-like expansion. Most displacement-based theories can be formulated on the basis of the above generic kinematic field. Classical beam models such as Timoshenko's (TBM) [19] and Euler-Bernoulli's (EBBM) [11] are easily derived from the linear expansion, $N = 1$ [5]. Models having constant and linear distributions of the in-plane displacements components, u_x and u_z, require opportunely reduced material coefficients to overcome Poisson's locking effect [3]. For the sake of brevity, the explicit expression for these coefficients is not reported here, but can be found in [4].

The FE approach is herein adopted to discretize the structure along the y axis. By introducing the shape functions N_i and the nodal displacement vector $\boldsymbol{q}$, the displacement field becomes:

$$\boldsymbol{u}\,(x,\,y,\,z) \;=\; F_\tau\,(x,\,z)\;N_i\,(y)\;\boldsymbol{q}_{\tau i} \qquad\qquad i = 1,\;2,\;\ldots,\;N_N \tag{7}$$

where $\boldsymbol{q}_{\tau i} = \left\{ q_{u_{x\tau i}} \quad q_{u_{y\tau i}} \quad q_{u_{y\tau i}} \right\}^T$ contains the degrees of freedom of the τ^{th} expansion term corresponding to the i^{th} element node. Elements with a number of nodes N_N equal to 4 are formulated and hereinafter referred as B4. A cubic approximation along the y axis is adopted [1].

The stiffness matrix of the elements is built via the Principle of Virtual Displacements:

$$\delta L_{int} \;=\; \int_V \left(\delta\boldsymbol{\varepsilon}_n^T\,\boldsymbol{\sigma}_n \;+\; \delta\boldsymbol{\varepsilon}_p^T\,\boldsymbol{\sigma}_p\right)\,dV \;=\; \delta L_{ext} \tag{8}$$

where L_{int} stands for the strain energy and L_{ext} is the work of external loadings. δ stands for virtual variation. By using Eqs. 3, 4, and 7 the internal virtual work becomes:

$$\delta L_{int} \;=\; \delta\boldsymbol{q}_{\tau i}^T\;\;\boldsymbol{K}^{ij\tau s}\;\boldsymbol{q}_{sj} \tag{9}$$

$\boldsymbol{K}^{ij\tau s}$ is the 3×3 *fundamental nucleus* of the structural stiffness matrix. For the sake of brevity, its explicit expression is not reported here, but it can be found in [20]. It should be noted that no assumptions on the expansion order have been made. Therefore, it is possible to obtain refined beam models without changing the formal expression of the nucleus components. Shear locking is corrected through selective integration [1].

4 STRUCTURAL AND AERODYNAMIC NOTATIONS

The proposed beam model can easily analyze non-planar wing configurations with arbitrary orientation in the 3D space, such as tapered wings with dihedals and sweep angles.

The aerodynamic method here chosen is the Vortex Lattice Method (VLM) [15]. The aerodynamic mesh, which consists in a lattice of N_{AP} quadrilateral panels, lies on a reference trapezoidal surface with 2 edges parallel to the wind direction. As shown in

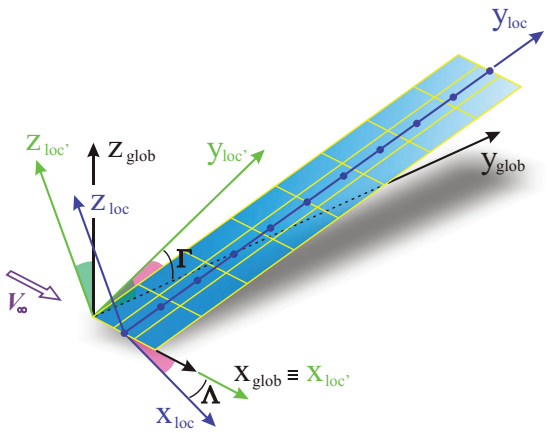

Figure 2: One-dimensional structural mesh and two-dimensional aerodynamic mesh of the wing structure.

Fig. 2, a second coordinate system $x_{\text{loc}'} - y_{\text{loc}'} - z_{\text{loc}'}$ is introduced so that the reference surface lies on the $x_{\text{loc}'} - y_{\text{loc}'}$ plane. A global coordinate system $x - y - z$ is placed on the airfoil's leading edge point at the root wing section so that x and $x_{\text{loc}'}$ axes are both parallel to the free stream velocity $\boldsymbol{V}_\infty$ (see Fig. 2).

The wing is modeled with a straight beam. The structural FE mesh is contained along the y_{loc} axis, which is on the trapezoidal reference surface. The fundamental nucleus (see Eq. 9) was derived in the local coordinate system. The notation is slightly modified by introducing the subscript "loc" to reflect this fact:

$$\delta L_{int} = \delta \boldsymbol{q}_{\tau i\,\text{loc}}^T \boldsymbol{K}_{\text{loc}}^{ij\tau s} \boldsymbol{q}_{sj\,\text{loc}} = \delta \boldsymbol{q}_{\tau i}^T \left[\boldsymbol{e}^T \cdot \boldsymbol{K}_{\text{loc}}^{ij\tau s} \cdot \boldsymbol{e} \right] \boldsymbol{q}_{sj} = \delta \boldsymbol{q}_{\tau i}^T \boldsymbol{K}^{ij\tau s} \boldsymbol{q}_{sj} \tag{10}$$

where $\boldsymbol{e}$ is the 3×3 rotation matrix relating the global and the local coordinate systems.

5 SPLINING AND AEROELASTIC FORMULATION

The present advanced beam model allows a very accurate calculation of the displacement field at any point of the three-dimensional wing. Based on this property, the Infinite Plate Spline method [8, 13] was shown (see [21]) to be the ideal choice for the aerodynamic load transferring with the advanced multi-fidelity beam model presented in this work. For the sake of brevity, the final expressions relating the displacements at aerodynamic load points and slopes at aerodynamic control points to the nodal DOFs vector of the whole structure are reported:

$$\widetilde{\boldsymbol{\mathcal{Z}}}_{\text{loc}'} = \widetilde{\boldsymbol{A}}_3^\star \cdot \boldsymbol{q} \qquad \frac{\mathrm{d}\boldsymbol{\mathcal{Z}}_{\text{loc}'}}{\mathrm{d}x_{\text{loc}'}} = \frac{\mathrm{d}\boldsymbol{\mathcal{Z}}_{\text{loc}'}}{\mathrm{d}x} = \boldsymbol{A}_3 \cdot \boldsymbol{q} \tag{11}$$

The coordinate system for the splining is the local′ one. More details about the adaptation of the IPS to the CUF-beam via a set of pseudo-structural points can be found in [21, 20]. The derivation of aerodynamic loads is now faced. According to the VLM [15], the

pressures acting on the wing are transferred as lift forces located on load points of the aerodynamic panels and perpendicular to the wind direction:

$$\boldsymbol{L} \;=\; \frac{1}{2}\,\rho_\infty\, V_\infty^2\, \boldsymbol{I}^D \cdot\; \Delta\boldsymbol{p} \;=\; \frac{1}{2}\,\rho_\infty\, V_\infty^2\, \boldsymbol{I}^D \cdot\; \left[\boldsymbol{A}^D\right]^{-1} \cdot\; \boldsymbol{w} \tag{12}$$

where $\Delta\boldsymbol{p}$ contains the dimensionless pressure acting on all the load points, normalized with respect to the dynamic pressure. $\boldsymbol{I}_D$ contains the panels' geometrical data. The VLM allows the dimensionless normalwash $\boldsymbol{w}$, normalized with respect to V_∞, to be described as a function of vector $\Delta\boldsymbol{p}$ by means of the Aerodynamic Influence Coefficient Matrix $\boldsymbol{A}^D$.

In the steady case, considering that the structure changes configuration when it deforms, the *boundary condition* used for the Vortex Lattice formulation imposes the dimensionless normalwash to equal the slope at the control points:

$$\boldsymbol{w} \;=\; \frac{\mathrm{d}\boldsymbol{\mathcal{Z}}_{\mathrm{loc}'}}{\mathrm{d}x_{\mathrm{loc}'}} \tag{13}$$

The transfer from loads at the aerodynamic points to the *energetically* equivalent loads at structural nodes is performed via the Principle of Virtual Displacements. All the lift forces are parallel to the $\boldsymbol{z}_{\mathrm{loc}'}$ axis, hence:

$$\begin{gathered}\delta W \;=\; \delta\widetilde{\boldsymbol{\mathcal{Z}}}_{\mathrm{loc}'}^{\,T} \cdot\; \boldsymbol{L} \;=\; \delta\boldsymbol{q}^T \cdot\; \widetilde{\boldsymbol{A}}_3^{\star\,T} \cdot\; \frac{1}{2}\,\rho_\infty\, V_\infty^2\, \boldsymbol{I}^D \cdot\; \left[\boldsymbol{A}^D\right]^{-1} \cdot\; \boldsymbol{A}_3 \cdot\; \boldsymbol{q} \;=\; \delta\boldsymbol{q}^T \cdot\; \boldsymbol{L}_{\mathrm{str}} \\ \Rightarrow \quad \boldsymbol{L}_{\mathrm{str}} \;=\; -\,\boldsymbol{K}_{\mathrm{aero}} \cdot\; \boldsymbol{q}\end{gathered} \tag{14}$$

where the negative sign is adopted for the sake of convenience. Such a term can go to the left hand side of the aeroelastic equation system and summed up to the structural stiffness matrix:

$$\boldsymbol{K}_{\mathrm{str}} \cdot\; \boldsymbol{q} \;=\; \boldsymbol{L}_{\mathrm{str}} \;=\; -\,\boldsymbol{K}_{\mathrm{aero}} \cdot\; \boldsymbol{q} \tag{15}$$

$$\Big[\,\boldsymbol{K}_{\mathrm{str}} \;+\; \boldsymbol{K}_{\mathrm{aero}}\,\Big] \cdot\; \boldsymbol{q} \;=\; \boldsymbol{0} \qquad\qquad \boldsymbol{K}_{\mathrm{aeroelastic}} \cdot\; \boldsymbol{q} \;=\; \boldsymbol{0} \tag{16}$$

where $\boldsymbol{K}_{\mathrm{aeroelastic}}$ is the aeroelastic stiffness matrix. The stiffness of the system now takes into account the aerodynamic loads due to the deformed configuration. From Eq. 16 it appears that there is no motion. It occurs because the angle of attack so far considered is zero. To solve this problem, a different from zero angle of attack is assigned to the wing and the corresponding aerodynamic lift forces acting on the panels are computed. The wall tangency condition is now imposed at the control point of each panel by setting the dimensionless normalwash to be equal to the local slope:

$$w \;=\; \tan\left(\pi - \alpha\right) \tag{17}$$

where the angle of attack α is a small quantity (linear aerodynamic model). Following the same procedure used to build $\boldsymbol{L}_{\mathrm{str}}$, the energetically equivalent nodal loads $\boldsymbol{L}_{\mathrm{RHS}}$ (the subscript RHS means Right Hand Side) are:

$$\boldsymbol{L}_{\mathrm{RHS}} \;=\; \frac{1}{2}\,\rho_\infty\, V_\infty^2\, \tan\left(\pi - \alpha\right)\, \widetilde{\boldsymbol{A}}_3^{\star\,T} \cdot\; \boldsymbol{I}^D\, \left[\boldsymbol{A}^D\right]^{-1} \boldsymbol{d} \tag{18}$$

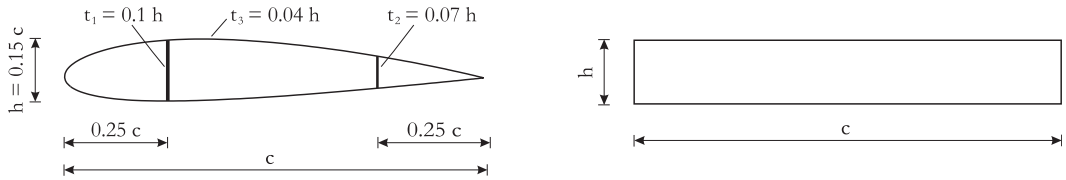

(a) NACA 2415 with 3 cells (b) Rectangular section

Figure 3: Cross-sections used for the wing configurations.

where $\boldsymbol{d}$ stands for a $N_{AP} \times 1$ vector of ones. More details about this procedure can be found in [20]. In conclusion, the final aeroelastic equation to be solved is:

$$\boldsymbol{K}_{\text{aeroelastic}} \cdot \boldsymbol{q} = \boldsymbol{L}_{\text{RHS}} \tag{19}$$

Equation 19 allows nodal displacement vector $\boldsymbol{q}$ to be computed. Now that the right hand side is different from zero, we have a solution.

6 RESULTS AND DISCUSSION

A number of wings with different geometries, layout and loadings are considered. Two different solutions are investigated and compared in this work. The first one coincides with the static structural analysis, hereinafter referred as SSA, and involves only the structural stiffness matrix by disabling the aerodynamic matrix $\boldsymbol{K}_{\text{aero}}$. The second solution is the static aeroelastic analysis (SAA) which solves the aeroelastic system (Eq. 19) by adding the aerodynamic stiffness matrix to the elastic one. Unless otherwise specified, the wings are subjected to a pure aerodynamic loading (vector $\boldsymbol{L}_{\text{RHS}}$). Cantilever boundary condition on half-wings is accounted for and the symmetry condition is exploited in the aerodynamic computation.

A swept tapered wing is first taken into account. A half-wing is modeled via a cantilever beam by using the following data: length $L = 5$ m, root chord $c_{root} = 1.6$ m, taper ratio $\lambda = 0.25$, and sweep angle $\Lambda = +13.5°$. The cross-section is a thin-walled NACA 2415 airfoil, which is subdivided into three cells by two longerons along the spanwise direction at 25% and 75% of the chord (see Fig. 3a). An isotropic aluminium (Young's modulus $E = 69$ GPa and Poisson's ratio $\nu = 0.33$) is considered.

A convergence study is carried out to evaluate the combined effect of the number of finite elements N_{EL} and the expansion order N on the solution. The mechanics of the beam is described in terms of the maximum vertical displacement $u_{z\,\max}$, which is located at the trailing edge of the tip cross-section. The results for SSA and SAA are shown in Tables 1 and 2, respectively. $u_{z\,\max}$ increases with N for any mesh, to such an extent that no remarkable differences are detected for high-order expansion. The numerical convergence on N_{EL} is achieved both for SSA and SAA. Linear theories EBBM, TBM, and $N = 1$ are unable to handle any torsional behavior. Poisson's locking correction is not sufficient to make them effective in computing the maximum displacement.

Table 1: Convergence study: effect of the number of $B4$ elements on $u_{z\,\max}$ [mm] for different beam models. Swept tapered wing. $V_\infty = 50$ m/s, $\alpha = 3°$, 4×40 panels. SSA.

N_{EL}	EBBM	TBM	$N = 1$	$N = 2$	$N = 3$	$N = 4$
2	4.2749	4.2829	4.2909	4.4309	4.9598	5.1036
5	3.1768	3.1842	3.1965	3.6408	3.8045	3.8858
10	3.0401	3.0473	3.0605	3.4701	3.5785	3.6316
20	3.0071	3.0144	3.0277	3.4097	3.4854	3.5377
40	2.9990	3.0062	3.0196	3.3920	3.4440	3.4802
	-13.69 %	-13.49 %	-13.10 %	-2.383 %	-0.886 %	+0.155 %

MD NASTRAN-solid (sol 101): 3.4748

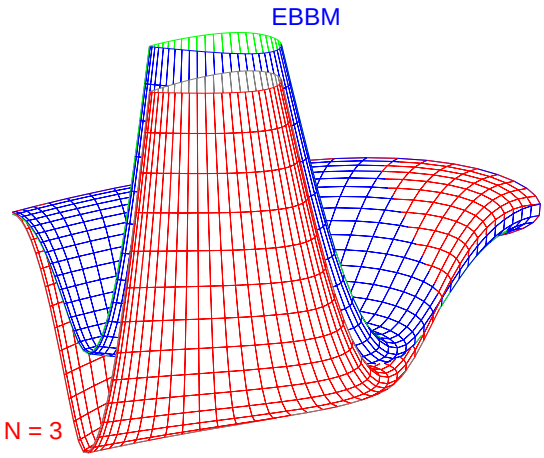

Figure 4: Tridimensional deformation of the swept tapered wing. $P_z = -7.2$ kN. SAA.

Table 2: Convergence study: effect of the number of $B4$ elements on $u_{z\,\max}$ [mm] for different beam models. Swept tapered wing. $V_\infty = 50$ m/s, $\alpha = 3°$, 4×40 panels. SAA.

N_{EL}	EBBM	TBM	$N = 1$	$N = 2$	$N = 3$	$N = 4$
2	4.2747	4.2827	4.2904	4.4236	4.9456	5.0915
5	3.1767	3.1841	3.1959	3.6307	3.7930	3.8743
10	3.0400	3.0472	3.0598	3.4597	3.5678	3.6206
20	3.0071	3.0143	3.0270	3.3993	3.4749	3.5269
40	2.9989	3.0061	3.0189	3.3816	3.4337	3.4695
	-13.40 %	-13.20 %	-12.83 %	-2.353 %	-0.849 %	+0.185 %

MD NASTRAN-shell (sol 144): 3.4631

On the contrary, as far as the SSA is concerned, the refined 1D models (5445 DOFs) are very close to MD NASTRAN-solid results (sol 101 - 10^6 DOFs). Besides, excellent agreement with aeroelastic MD NASTRAN-shell results (sol 144 - 2135 DOFs) is obtained for the aeroelastic analysis (SAA). Figure 3 shows the tridimensional deflection of the wing, drawn by means of a large scale factor, if a bending force ($P_z = -7.2$ kN) is combined to the aerodynamic load. The third-order model clearly illustrates the torsional effect, whereas the limits of EBBM are once again made evident.

Table 3: Effect of the free stream velocity V_∞ [m/s] on $u_{z\,\max}$ [mm]. Unswept wing with rectangular section. 20 B4 elements. $\alpha = 1°$, 10×50 panels. SSA vs SAA.

	$V_\infty = 30$		$V_\infty = 50$		$V_\infty = 70$	
	SSA	SAA	SSA	SAA	SSA	SAA
$EBBM$	68.650	68.611	190.693	190.398	373.756	372.628
	-0.05573 %		-0.15459 %		-0.30189 %	
$N = 2$	62.640	68.236	173.999	224.454	341.038	599.986
	+8.93451 %		+28.99720 %		+75.92906 %	
$N = 4$	66.947	73.397	185.963	244.464	364.487	668.562
	+9.63479 %		+31.4584 %		+83.42555 %	

Table 4: Effect of tailoring on the twist $\Delta u_{z\ TIP}$ [mm] of the tip cross-section. Unswept wing with rectangular section. 20 B4 elements. $V_\infty = 50$ m/s, $\alpha = 1°$, 10×50 panels. Orthotropic material. SSA vs SAA.

θ	SSA $N = 4$	SAA $N = 4$	SAA NASTRAN	SAA % Diff
$-60°$	2.9935	3.5297	3.5407	-0.3107
$-30°$	4.3186	5.5433	5.5408	$+0.0451$
$0°$	1.0209	1.0708	1.0741	-0.3072
$30°$	-2.4578	-2.1753	-2.1638	$+0.5315$
$60°$	-1.1199	-1.0576	-1.0439	$+1.3124$
$90°$	1.0396	1.0914	1.1065	-1.3647

An unswept wing of length $L = 5$ m with a rectangular cross-section is introduced. Referring to Fig. 3b, the chord c is equal to 1 m and the height is $h = 20$ mm. Table 3 reports a parametric study on $u_{z\,\max}$, placed at the leading edge of the tip cross-section,

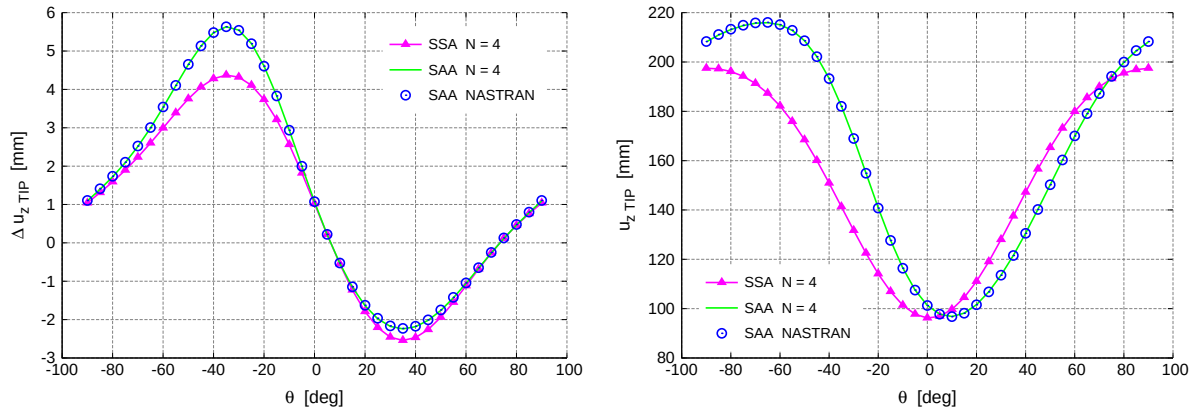

(a) Twist (b) Bending

Figure 5: Effect of tailoring on the twist and bending of the tip cross-section. Unswept wing with rectangular section. Orthotropic material. SSA vs SAA.

as the free stream velocity changes. While $u_{z\,\max}$ increases linearly with the square of V_∞ for SSA, the same does not occur for SAA. The contribution of $\boldsymbol{K}_{\text{aero}}$ to system stiffness becomes more evident as V_∞ increases and the difference from SSA can become very significant for $V_\infty = 70$ m/s. This difference increases with the expansion order N, which enhances the flexibility of the structure. EBBM is ineffective in describing the difference between structural and aeroelastic behavior.

The length L of the unswept wing is further extended to 10 m. The chord c is equal to 1 m and the height of the rectangular section is $h = 100$ mm. A composite material is introduced to analyze the well-known aeroelastic tailoring. Young's modulus along the longitudinal axis E_L is equal to 20.5 GPa, whereas those along the transverse directions are equal to 10 GPa. Poisson's ratio $\nu = 0.25$ and the shear modulus $G = 5$ GPa are the same in all directions. Table 4 shows the effect of the lamination θ on the torsion of the tip cross-section due to the only aerodynamic pressure. The quantity Δu_z is defined as the difference of u_z between leading and trailing edges. The aeroelastic tailoring is more evident for the wing twist evaluation as it is presented in Fig. 5a.

The comparison of SSA and SAA underlines the importance of the contribution of $\boldsymbol{K}_{\text{aero}}$ in the case $N = 4$ to evaluate the aeroelastic behavior of composite wings. While the curve related to SSA is essentially symmetrical with respect to the $\theta = 0°$ lamination, the aeroelastic analysis shows a trend which is far from symmetrical. In general, the aeroelastic analysis leads the twist of the unswept wing to be higher compared to the structural solution as the lamination changes, expecially for negative values of θ. The same result occurs for bending behavior as shown in Fig. 5b, where only the SSA case obtains an almost symmetrical curve. The excellent agreement between the fourth-order beam model and MD NASTRAN-shell (sol 144) to describe the aeroelastic response of orthotropic wings with generic orientation is again striking.

7 CONCLUSIONS

This paper has extended the Vortex Lattice Method and a refined one-dimensional structural model for the analysis of anisotropic wings. Advanced 1D finite elements have been obtained via the Carrera Unified Formulation which allows any order theory to be obtained in a hierarchical manner. The static aeroelastic and structural response of wings with different geometries and cross-sections has been analyzed. Isotropic and composite materials has been considered.

The CUF-VLM structural and coupling models have been assessed and compared with MD NASTRAN results. The effectiveness of higher-order models for an accurate analysis of aircraft wings exposed to a free stream has been shown in respect to classical theories. Comparison of structural and aeroelastic solutions has underlined the importance of the contribution of aerodynamic stiffness. The effect of aeroelastic tailoring has been investigated and excellent agreement with MD NASTRAN in evaluating the aeroelastic response of composite wings has been documented. Future works will focus on aeroelastic static and dynamic stability analyses (divergence and flutter).

REFERENCES

[1] K.J. Bathe. *Finite element procedure*. Prentice hall, Upper Saddle River, New Jersey, 1996.

[2] E. Carrera. Theories and finite elements for multilayered plates and shells: a unified compact formulation with numerical assessment and benchmarking. *Archives of Computational Methods in Engineering*, 10(3):216–296, 2003.

[3] E. Carrera and S. Brischetto. Analysis of thickness locking in classical, refined and mixed multilayered plate theories. *Composite Structures*, 82(4):549–562, 2008.

[4] E. Carrera and G. Giunta. Refined beam theories based on a unified formulation. *International Journal of Applied Mechanics*, 2(1):117–143, 2010.

[5] E. Carrera, G. Giunta, P. Nali, and M. Petrolo. Refined beam elements with arbitrary cross-section geometries. *Computers and Structures*, 88(5–6):283–293, 2010. DOI: 10.1016/j.compstruc.2009.11.002.

[6] E. Carrera, M. Petrolo, and A. Varello. Advanced beam formulations for free vibration analysis of conventional and joined wings. *Journal of Aerospace Engineering*, 2010. In press.

[7] L. Demasi. ∞^3 hierarchy plate theories for thick and thin composite plates: the generalized unified formulation. *Composite Structures*, 84(3):256–270, 2008.

[8] L. Demasi and E. Livne. Dynamic aeroelasticity of structural nonlinear configurations using linear modally reduced aerodynamic generalized forces. *AIAA Journal*, 47(1):71–90, 2009.

[9] E.H. Dowell and K.C. Hall. Modeling of fluid-structure interaction. *Annual Review of Fluid Mechanics*, 33:445–490, 2001.

[10] R. El Fatmi. Non-uniform warping including the effects of torsion and shear forces. Part I: A general beam theory. *International Journal of Solids and Structures*, 44(18-19):5912–5929, 2007.

[11] L. Euler. *De curvis elasticis*. Bousquet, Lausanne and Geneva, 1744.

[12] Y.C. Fung. *An Introduction to the Theory of Aeroelasticity*. Dover Publications, 2008.

[13] R. Harder and R.N. Desmarais. Interpolation using surface splines. *Journal of Aircraft*, 9(2):189–192, 1972.

[14] K. Kapania and S. Raciti. Recent advances in analysis of laminated beams and plates, part I: Shear effects and buckling. *AIAA Journal*, 27(7):923–935, 1989.

[15] J. Katz and A. Plotkin. *Low-Speed Aerodynamics*. Cambridge University Press, 2001.

[16] L. Librescu and O. Song. On the static aeroelastic tailoring of composite aircraft swept wings modelled as thin-walled beam structures. *Composites Engineering*, 2:497–512, 1992.

[17] J.N. Reddy. *Mechanics of laminated composite plates and shells. Theory and Analysis*. CRC Press, 2^{nd} edition, 2004.

[18] N. Silvestre and D. Camotim. First-order generalised beam theory for arbitrary orthotropic materials. *Thin-Walled Structures*, 40(9):791–820, 2002.

[19] S.P. Timoshenko and J.N. Goodier. *Theory of elasticity*. McGraw-Hill, New York, 1970.

[20] A. Varello, E. Carrera, and L. Demasi. Vortex lattice method coupled with advanced one-dimensional structural models. *Journal of Aeroelasticity and Structural Dynamics*, 2011. Submitted.

[21] A. Varello, L. Demasi, E. Carrera, and G. Giunta. An improved beam formulation for aeroelastic applications. In *51st AIAA/ASME/ASCE/AHS/ASC Structures, Structural Dynamics, and Materials Conference*, AIAA Paper 2010-3032, Orlando, Florida, 12-15 April 2010.

[22] W. Yu, V.V. Volovoi, D.H. Hodges, and X. Hong. Validation of the variational asymptotic beam sectional analysis (VABS). *AIAA Journal*, 40(10):2105–2113, 2002.